Magnetic Resonance in Medicine 50:1120–1126 (2003)

Amide Proton Transfer (APT) Contrast for Imaging of Brain Tumors

Jinyuan Zhou,[1,2*] Bachchu Lal,[3] David A. Wilson,[4] John Laterra,[3,5–7] and Peter C.M. van Zijl[1,2*]

In this work we demonstrate that specific MR image contrast can be produced in the water signal that reflects endogenous cellular protein and peptide content in intracranial rat 9L gliosarcomas. Although the concentration of these mobile proteins and peptides is only in the millimolar range, a detection sensitivity of several percent on the water signal (molar concentration) was achieved. This was accomplished with detection sensitivity enhancement by selective radiofrequency (RF) labeling of the amide protons, and by utilizing the effective transfer of this label to water via hydrogen exchange. Brain tumors were also assessed by conventional T_1-weighted, T_2-weighted, and diffusion-weighted imaging. Whereas these commonly-used approaches yielded heterogeneous images, the new amide proton transfer (APT) technique showed a single well-defined region of hyperintensity that was assigned to brain tumor tissue. Magn Reson Med 50:1120–1126, 2003. © 2003 Wiley-Liss, Inc.

Key words: amide proton exchange; mobile protein; peptide; magnetization transfer; 9L gliosarcoma

Although many types of cells contain an abundance of proteins and peptides, these molecules do not provide intense signals in proton magnetic resonance spectroscopy (MRS) experiments, and they have been rarely examined in vivo or in cells (1–3). At present, there are no MRI methods available to spatially assess proteins and peptides in vivo. However, many cellular activities are performed by proteins, and various lesions, such as those found in tumors and stroke, may show changes in the concentration and properties of proteins and peptides. Information at the protein level may be relevant for earlier detection, better spatial definition, and improved characterization of diseases (3,4). Behar and Ogino (1) and Kauppinen et al. (2) first detected and identified several macromolecular peaks in the low-frequency range (0–4 ppm) of brain proton magnetic resonance (MR) spectra. These signals were attributed to contributions from mobile proteins, polypeptides, and lipids. The backbones of proteins and peptides have amide resonances in the high-frequency range (~8 ppm) of the proton spectrum (5). Recently, Mori et al. (6) observed the presence of a composite resonance at ~8.3 ± 0.5 ppm in the in situ proton spectra of cancer cells and cat brain, the signal intensity of which was sensitive to pH changes. Using a rat brain water exchange (WEX) experiment, we recently verified (7) that the composite resonance at 8.3 ppm is from the amide protons of cellular proteins and peptides. We also observed the pH-dependent in situ exchange effect with bulk water protons following cardiac arrest. The exchange rates measured were in accordance with knowledge gained from in vitro protein high-resolution MRS studies. The 8.3 ppm resonance was also reported in human brain proton spectra at 4 T by Chen and Hu (8).

To increase MR detection sensitivity, it would be useful to be able to detect protein and peptide signals indirectly via the water resonance, especially for imaging purposes. Because there is exchange between amide protons of intracellular mobile proteins and peptides and the water protons, this is indeed possible. In recent studies using small molecules in solution, Wolff and Balaban (9) and Ward et al. (10) proposed the use of a chemical exchange saturation transfer (CEST) enhancement scheme, and demonstrated that the process of saturation transfer from exchangeable protons to water could be used for metabolite sensitivity enhancement. Subsequently, large enhancements in sensitivity (up to 500000 (11)) were demonstrated for amide protons of cationic polymers (poly-lysine, dendrimers), which have a favorable exchange rate range (10–300 s^{-1}) for effective selective irradiation and chemical exchange transfer under physiological conditions. These results suggested that detection sensitivity enhancement through selective saturation transfer via water-exchangeable amide protons of mobile proteins and peptides in biological tissue may allow spatial assessments of amide proton content and properties via the water signal. We recently demonstrated such amide proton transfer (APT) effects in rat brain and applied APT imaging to map pH effects in rat brain during ischemia (12). In this work, we demonstrate that this new imaging modality can be used to detect brain tumors, predominantly on the basis of their higher protein/peptide content compared to brain tissue.

MATERIALS AND METHODS

Theory

With the use of a two-site exchange model (a small pool for protein/peptide amide protons and a large pool for bulk

[1]Department of Radiology, Johns Hopkins University School of Medicine, Baltimore, Maryland.
[2]F.M. Kirby Research Center for Functional Brain Imaging, Kennedy Krieger Institute, Baltimore, Maryland.
[3]Department of Neurology, Kennedy Krieger Institute, Baltimore, Maryland.
[4]Department of Anesthesiology, Johns Hopkins University School of Medicine, Baltimore, Maryland.
[5]Department of Neurology, Johns Hopkins University School of Medicine, Baltimore, Maryland.
[6]Department of Oncology, Johns Hopkins University School of Medicine, Baltimore, Maryland.
[7]Department of Neuroscience, Johns Hopkins University School of Medicine, Baltimore, Maryland.

Grant sponsor: NIH/NINDS; Grant number: NS31490; Grant sponsor: NIH/NIBIB; Grant number: EB02666; Grant sponsor: Whitaker Foundation.

*Correspondence to: Jinyuan Zhou or Peter van Zijl, Division of MRI Research, Department of Radiology, Johns Hopkins University School of Medicine, 217 Traylor Building, 720 Rutland Ave., Baltimore, MD 21205-2195. E-mail: jzhou@mri.jhu.edu

Received 2 June 2003; revised 13 August 2003; accepted 13 August 2003.
DOI 10.1002/mrm.10651
Published online in Wiley InterScience (www.interscience.wiley.com).

© 2003 Wiley-Liss, Inc.

water protons), and assuming complete amide proton saturation under selective radiofrequency (RF) irradiation, the proton transfer ratio (*PTR*) for the amide protons (*APTR*) in the water signal can be derived to be (11,12):

$$APTR = \frac{k[\text{amide proton}]}{[\text{water proton}]R_{1w}}(1 - e^{-R_{1w}t_{sat}}) \qquad [1]$$

where k is the normalized proton exchange rate between the two proton pools, square brackets ([. . .]) denote concentration, R_{1w} is the spin-lattice relaxation rate of water, and t_{sat} is the length of the saturation time. Equation [1] indicates that the APT effects are sensitive to the water content of tissue, w ([water proton] = 2 × 55 M × w), and in order to be distinguishable from conventional image contrast, the effects of amide proton content and/or exchange must be substantially different from the other terms.

In conventional magnetization transfer (MT) experiments (13–15), RF saturation effects on water in tissue are often plotted as a function of saturation frequency offset relative to water (the so-called *z*-spectra). It is not straightforward to demonstrate APT effects superimposed on the large saturation transfer effects between solid-like macromolecules and cellular water. In addition, APT effects occur at ~8.3 ppm (i.e., close to the water frequency), and direct water saturation effects will also interfere, especially at low magnetic fields. Because the shape of the direct water saturation region of the *z*-spectra depends on T_{2w} and T_{1w}, changes in blood oxygen level-dependent (BOLD) effects or water content will also influence the APT region. To selectively assess APT effects without interference from conventional MT, direct water saturation, or BOLD effects, it is useful to define an asymmetry parameter by subtracting the MT ratios ($MTR = 1 - S_{sat}/S_0$) obtained at the negative offset with respect to water from those at the corresponding positive offset (12):

$$\begin{aligned} MTR_{asym} &= MTR(+\text{offset}) - MTR(-\text{offset}) \\ &= S_{sat}/S_0(-\text{offset}) - S_{sat}/S_0(+\text{offset}) \end{aligned} \qquad [2]$$

where S_{sat} and S_0 are the imaging signal intensities measured with and without RF saturation, respectively. If the conventional MT effects were symmetric with respect to the water resonance, any contribution due to proton exchange would result in a positive MT difference. However, the solid-like MT effect is asymmetric with respect to the water resonance (12,16), with a center frequency in the aliphatic range. As a consequence, the resulting MTR_{asym} curve for offsets 0–5 ppm from water has an offset-dependent shape that depends on the inherent MTR_{asym} of the solid-phase MT effect (MTR'_{asym}) as well as on the *PTR* of the contributing exchangeable protons:

$$MTR_{asym}(\text{offset}) = MTR'_{asym}(\text{offset}) + PTR(\text{offset}). \qquad [3]$$

In a comparison of lesions or physiological alterations, the change in MTR_{asym}, ΔMTR_{asym}, equals the change in *PTR*, ΔPTR, under the assumption of an unaltered MTR'_{asym}. Therefore, *PTR* at the 3.5 ppm offset (*APTR*), which corresponds to the 8.3 ppm resonance in the proton spectrum, can be assessed under the assumption that MTR'_{asym} (3.5 ppm) remains unaltered.

Animal Preparation

The animals were cared for throughout the experimental procedures in accordance with institutional guidelines. Nine Fischer 344 rats weighing 200–250 g were anesthetized by intraperitoneal injection of 0.2 ml/100 g body weight of 25 mg/ml of xylazine and 2.5 mg/ml of ketamine. Through a small burr hole, 9L cells (25000 in 2 μl) were stereotaxically implanted (17) into the forebrain of the animal on the right side (3 mm lateral to bregma and 3 mm deep). On the postimplantation days indicated, the animals were reanesthetized with sodium pentobarbital (40 mg/kg, i.p.). A cannula was placed in the femoral vein to infuse anesthesia during MR procedures. The trachea was exposed through a midline incision, and a tracheotomy was performed to maintain a patent airway. The rat head was fixed with ear bars and taped to the coil and cradle to avoid motion artifacts. Body temperature was monitored and maintained at 37.5°C ± 0.5°C using a heating pad. During the MR experiments, a continuous infusion of dilute sodium pentobarbital in saline was infused by infusion pump (15 mg/kg/hr, i.v.). At the end of the study, the anesthetized rat was killed by an intravenous injection of KCl, and the brain was then excised and sectioned. Histologic sections (10 μ thick) were stained with hematoxylin and eosin.

MRI Experiments

Experiments were performed on a horizontal bore 4.7 T GE CSI animal imager. A surface coil (inner diameter = 3 cm) was used for RF transmission and reception. The pulse sequence used for APT imaging is the same as that used in the standard MT sequence, but we were interested in the amide proton exchange effects in a small offset range (1–5 ppm) above the water frequency. A train of 400 Gaussian pulses (length = 6.6 ms, flip angle = 180°, delay = 3.4 ms, total duration = 4 s, average RF power = ~50 Hz) was used for off-resonance RF irradiation (Fig. 1). The image slice was located at the level of the caudate nucleus. Slice shimming was done. Four-shot, spin-echo echo-planar imaging (EPI) was used for data acquisition (TR = 10 s, TE = 30 ms). The imaging matrix was 64 × 64, FOV was 40 × 40 or 32 × 32 mm^2, and the imaging slice thickness was 2 mm.

Two types of experiments were performed. In the first type, standard *z*-spectra were acquired over an offset range of ±7 ppm with a resolution of 0.5 ppm. One image was acquired per offset. The effects of the saturation transfer of exchangeable protons to water were subsequently identified by asymmetry analysis and comparison with normal brain. In the second type of experiment, APT-weighted images were acquired using only frequency-labeling offsets of ±3.5 ppm with respect to water (16 scans), followed by asymmetry (difference) analysis as in the first experiment. In addition to these APT experiments, several conventional imaging experiments were run, including diffusion (TR = 3 s, TE = 80 ms, 10 *b*-values = 0–1392 s/mm^2, 8 scans, single-shot trace diffusion weighting (18)), T_1

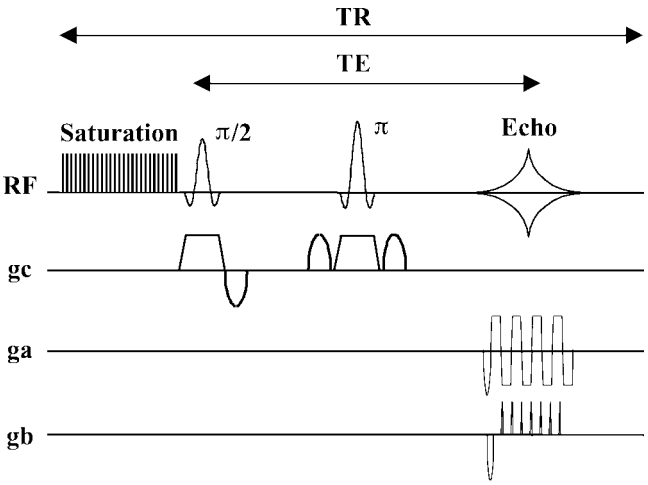

FIG. 1. APT imaging pulse sequence using a spin-echo EPI acquisition and a pulse train saturation scheme. A train of 400 Gaussian pulses (length = 6.6 ms, flip angle = 180°, delay = 3.4 ms, total duration = 4 s, average RF power = ~50 Hz) was used for off-resonance RF irradiation.

(TR = 2 s; TE = 30 ms; TI = 0.2, 0.6, 1.25, 1.6, 2, 2.5, and 3.4 s), and T_2 (TR = 2 s; TE = 25, 35, 45, 55, 65, 75, and 85 ms). About 2 hr were required to run these five sequences.

Data Processing

The measured imaging signal intensities (normalized with respect to unsaturated) as a function of offset (i.e., *z*-spectra) were fitted through all offsets using a 12th-order polynomial on a pixel-by-pixel basis. The actual water resonance was assumed to be at the frequency with the lowest signal intensity of the interpolated fitted curve using an offset resolution of 1 Hz. After fitting, the experimentally measured MT curve for each pixel was shifted correspondingly along the direction of the offset axis, which corrects for field inhomogeneity effects. The spin-lattice relaxation time of water, T_{1w}, was fitted with a three-parameter equation: $I = A + B \exp(-TI/T_{1w})$. T_{2w} was fitted using $I = I_0 \exp(-TE/T_{2w})$. The average apparent diffusion coefficient of water, $ADC_{av} = Trace(D)/3$, was fitted by $I = I_0 \exp(-b \cdot ADC_{av})$. The water content map was calculated from the T_{1w} map by using the empirical relationship $R_{1w} = 1/T_{1w} = \alpha(\frac{1}{w} - 1)$, in which the coefficient α was determined by T_{1w} and the average tissue water content (0.84 ml water/ml brain (19)) for the contralateral normal brain region. The same proportionality constant α was used for all tissues, while the T_{1w} values of individual tissues were used to determine the water content map on a pixel-by-pixel basis. When we calculated the amide proton concentration (Eq. [1]), we assumed negligible effects of the amide proton concentration on the exchange rate, and the value that was determined previously for normal brain tissue (28.6 s^{-1} (12)) was used for brain and tumor tissue.

RESULTS

Figure 2a shows *z*-spectra for tumor, peritumoral tissue, and contralateral normal tissue for the 9L brain tumor

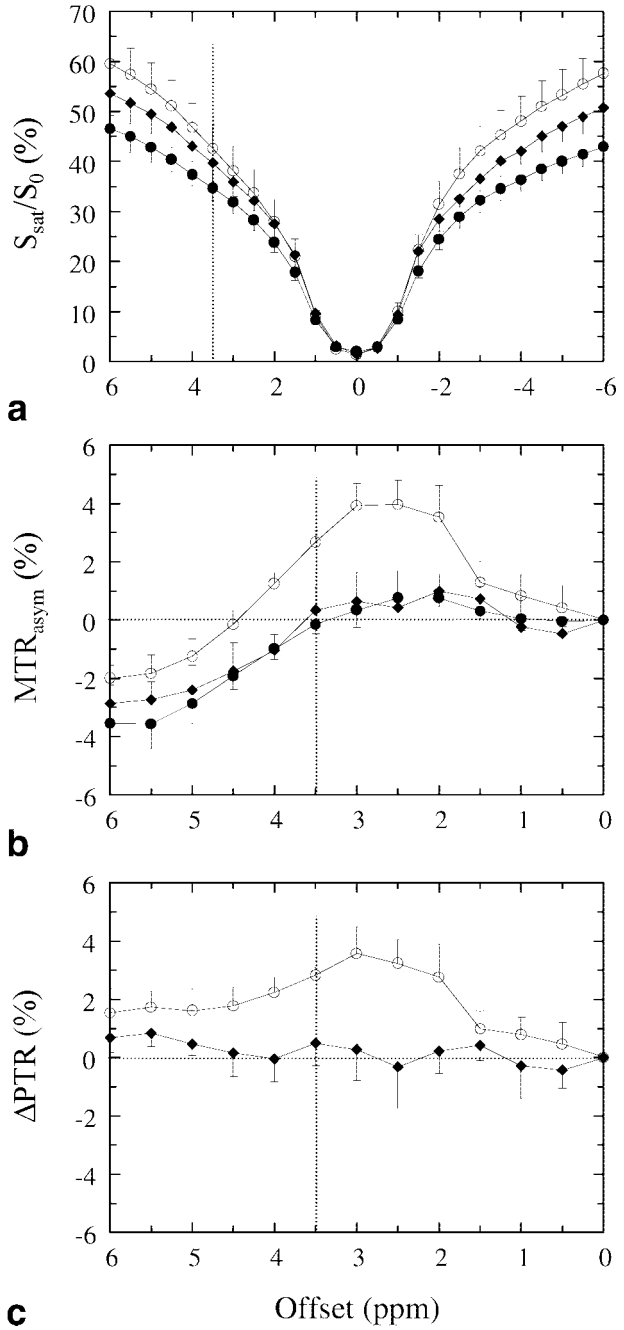

FIG. 2. *z*-spectra (**a**), MTR_{asym} spectra (**b**), and Δ*PTR* spectra (**c**) for the tumor-implanted rat brain (10 or 11 days; $N = 5$). Solid circle: contralateral region; diamond: peritumoral tissue; open circle: tumor. The *z*-spectra show the saturation of the water resonance as a function of RF irradiation frequency with respect to water. Signal attenuation is due mainly to direct water saturation close to the water frequency and the solid-like MT effect over the whole spectral range. Notice that the *z*-spectra are asymmetric, and when one compares the positive and negative offsets in the 2–3.5 ppm region, there are noticeable drops on the positive side. The MTR_{asym} spectra and Δ*PTR* spectra show that tumor changes are only visible in the 2–3.5 ppm offset range from water, corresponding to the exchangeable-proton range in the spectra.

model in rats (10 or 11 days postimplantation; $N = 5$). These three regions of interest (ROIs) were selected according to the calculated ADC_{av} maps and APT-weighted images. Peritumoral tissue, which may include edema and/or angiogenesis (20–25), was identified as a region surrounding the tumor with increased ADC_{av} and approximately normal MTR_{asym} (3.5 ppm). The shift of the *z*-spectrum as a result of field inhomogeneity depends on shimming. In our experiments, shimming was better than 25 Hz, and the shift values were within ±20 Hz for most brain regions, but could be larger for some pixels. The imaging signal intensities in the *z*-spectra are substantially reduced for all tissues, which is due to the effects of direct water saturation close to the water frequency, and of conventional MT over the whole spectral range. The *z*-spectrum differences for these three types of tissue are very clear; however, some of these may be due to changes in relaxation times that narrow the direct saturation curve. The effects of direct saturation and conventional MT are largely reduced in the MTR_{asym} spectrum in Fig. 2b, which shows a substantial increase in the tumor MTR_{asym} compared to the contralateral normal tissue. Notice that the range of offsets over which this increase occurs corresponds closely to the spectral range of exchangeable protons for proteins and peptides. This effect is also clear in the ΔPTR spectra with respect to normal tissue ($\Delta PTR = PTR$ (tumor or peritumoral tissue) – PTR (normal tissue)), which are given in Fig. 2c.

Figure 3 compares APT-based imaging with several conventional MR image types, including a T_{2w}-weighted image, a fitted T_{2w} map, a T_{1w}-weighted image, a fitted T_{1w} map, a diffusion-weighted image, and a calculated ADC_{av} map. These images show regions of increased T_{1w}, T_{2w}, and ADC_{av} in the tumor, which in many cases are surrounded by additional areas of even higher intensity. Overall, the tumor appears diffuse, with unclear regional boundaries. The same is true for the S_{sat}/S_0 images at the ±3.5 ppm offsets from water (and thus for standard MT images) and for the water content image. However, when one examines the APT-weighted image and the amide proton concentration map, a clearly outlined area becomes visible, which we interpret as originating predominantly from tumor tissue. A histological section shows that the tumor has well defined boundaries; however, since the histological section is much thinner than the MRI slice, no specific conclusions can be drawn regarding the accuracy of the boundaries seen in the APT-based images. Moreover, EPI acquisitions can lead to a distortion in the MR images, which makes it even more difficult to match the results with histology.

A comparison of the MRI parameters for the tumor, peritumoral, and normal tissue is given in Table 1 ($N = 5$). The results indicate the following properties for this type of brain tumor: 1) T_{2w}-weighted image hyperintensity or increased T_{2w}, 2) T_{1w}-weighted image hypointensity or increased T_{1w}, 3) diffusion-weighted image hypointensity or increased ADC_{av}, and 4) increased MTR_{asym} (3.5 ppm) and amide proton concentration (71.9–140.8 mM). The contralateral $APTR$ (2.94%) and amide proton concentration (71.9 mM) were those measured for normocapnic rat brain tissue in our previous in vivo/postmortem rat studies (12). These values were validated because they have *z*- and MTR_{asym} spectra that are comparable to those obtained in the contralateral hemisphere in the present study. Using the APT images as a basis for defining a well-contrasted area of tumor, we assigned regions as being peritumoral when they exhibited increased ADC_{av} and approximately normal MTR_{asym} (3.5 ppm). These peritumoral regions also showed markedly increased T_{2w} and T_{1w} with respect to normal brain.

DISCUSSION

Although MRI is universally applied for the diagnosis and therapeutic monitoring of various cerebral lesions, it remains difficult to accurately delineate brain tumor borders by several common types of MR images, such as T_{2w}-weighted, T_{1w}-weighted, and diffusion-weighted images. This may be due, in part, to the fact that these conventional imaging techniques often indicate very similar properties, such as increased water content or freedom of mobility, for a tumor and the surrounding edema (26–28), and thus there is a lack of MRI contrast by which to differentiate them. In addition, the presence of cerebrospinal fluid (CSF), which has longer relaxation times and higher ADC_{av}, may worsen the definition of tumor boundaries adjacent to CSF regions. In Gd-enhanced imaging, only the tumor area where the blood–brain barrier is broken is visible; however, the tumor may extend beyond this area, making treatment planning problematic. Thus, other contrast mechanisms that better reflect the properties of tumor tissue are urgently needed (29,30). In the present study we explored a recently developed method, termed APT imaging (12), that is based on our recent spectroscopy studies (5,7) in which a large resonance for backbone amide protons was found at a spectral frequency of 8.3 ppm (~3.5 ppm offset from water). This technology was hypothesized to be potentially useful for tumor identification.

Identifying APT

The APT effect occurs in addition to conventional MT contrast associated with immobile macromolecules and membranes, which is effective over a large spectral range (about 100–200 kHz) and is usually measured by saturating at offsets of 5–10 kHz (13–15). In the case of APT-based contrast, the irradiation offset to water ranges from about 2 to 5 ppm, corresponding to 400–1000 Hz at a field strength of 4.7 T. At this close proximity to water, as shown in Fig. 2a, signal attenuation due to direct water saturation is comparable with the conventional solid-based MT effect over the whole spectral range. Thus, the noticeable upward shift of the S_{sat}/S_0 curves for the tumor and peritumoral tissue with respect to normal brain can be attributed to these two effects, including relaxation-time effects on the shape of the direct saturation curve. This upward change in shape agrees with earlier reports of decreased MTR values in tumors and adjacent tissue (edema) when compared to normal brain tissue (20,21). On the other hand, APT-weighted imaging is dominated by the transfer effects from exchangeable amide protons of mobile cellular proteins and peptides to water protons in a narrow offset range (0–5 ppm). Several interesting features

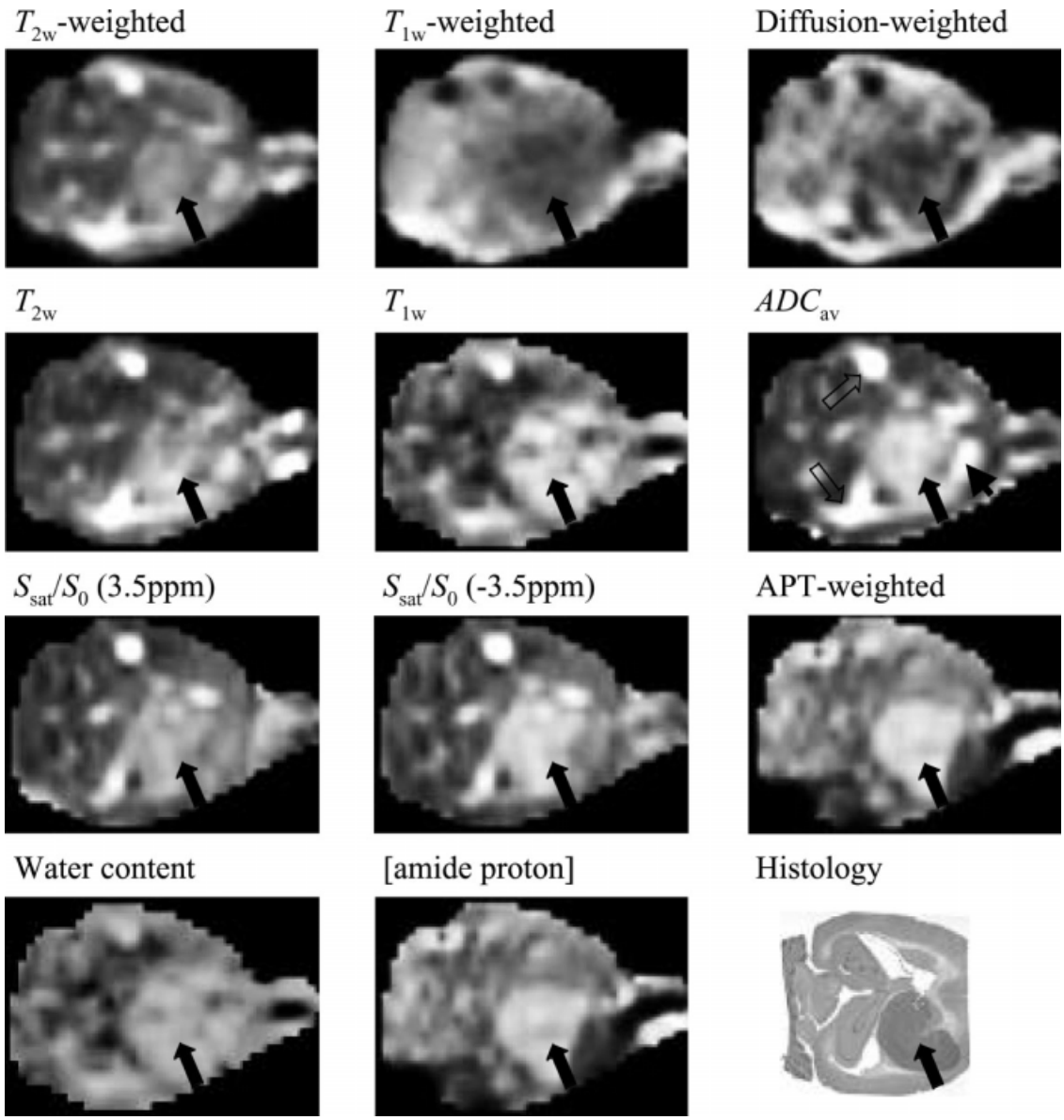

FIG. 3. Comparison of APT images with several common types of MR images and histology for a rat brain tumor. The conventional MR images include a T_{2w}-weighted image (TR = 3 s, TE = 80 ms, 8 scans), T_{2w} map, T_{1w}-weighted image (TR = 1 s, TE = 25 ms, 8 scans), T_{1w} map, isotropic diffusion-weighted image (TR = 3 s, TE = 80 ms, *b*-value = 1392 s/mm^2, 8 scans), and ADC_{av} map. The APT images include the MTR_{asym} (3.5 ppm) (i.e., APT-weighted) image and an amide proton content map. The APT-weighted image was obtained by subtracting the S_{sat}/S_0 images acquired at frequency-labeling offsets of ±3.5 ppm (16 scans), which are also displayed. Notice that the hyperintensity peritumoral tissue (arrowhead) and CSF (open arrow) in the ADC_{av} map (also the S_{sat}/S_0 (± 3.5 ppm) images) become normal in the APT-weighted image. The tumor is visible in all of the MR images (arrow), but its contour is much clearer in the APT images.

have been identified that support the existence of APT effects. For example, the *z*-spectra in Fig. 2a show a smaller intensity difference on the positive-offset side of water (2–3.5 ppm), where the exchangeable protons resonate, than on the negative-offset side. This agrees with the notion that increased protein/peptide content in tumor (3) leads to an increased saturation transfer (Eq. [1]), thus decreasing the imaging signal intensities.

The measured asymmetry curves (Fig. 2b) show an MTR_{asym} difference that is slightly positive at first and becomes negative at a higher offset. This result again supports a previous report (16) that the MT effect is asymmetric with respect to the water resonance, with a center frequency in the aliphatic range. The resulting curve for offsets 0–5 ppm from water has an offset-dependent shape that depends on the inherent asymmetry of the solid-phase MT effect (i.e., MTR'_{asym}), as well as on the *PTR* of the contributing exchangeable protons. When the tumor MTR_{asym} plot is subtracted from the contralateral curve (Fig. 2c), a maximum change in tumor signal intensity is found at offsets of 2–3.5 ppm from water. This corresponds to the middle of the frequency range of the amide protons in high-resolution protein and peptide spectra. As regards the proton spectral frequencies, the backbone amide pro-

Table 1
Measured MR Parameters for the 9L Brain Tumor (n = 5)

	T_{1w}(s)	T_{2w}(ms)	ADC_{av} (10^{-9}m/s)	MTR_{asym} (3.5ppm)	APTR	[a.p.] (mM)
Contralateral	1.40 ± 0.10	55.0 ± 5.5	0.82 ± 0.03	0.28 ± 0.49%	2.94%*	71.9*
Peritumoral	1.67 ± 0.07	86.5 ± 8.1	1.22 ± 0.18	−0.15 ± 0.55%	2.38 ± 0.77%	51.7 ± 16.3
Tumor	1.83 ± 0.17	63.8 ± 4.5	1.18 ± 0.09	4.11 ± 1.11%	6.77 ± 0.92%	140.8 ± 21.4

*The contralateral *APTR* and related amide proton concentration were obtained from the previous in vivo postmortem rat brain studies (12). Peritumoral regions were defined based on increased ADC_{av} and approximately normal MTR_{asym} (3.5 ppm).

tons are known to resonate around 8 ppm, and the flexible side chains have a composite amide resonance of ~6.8 ppm (5,7), corresponding well to the offset range (2–3.5 ppm) over which the signal changes shown in Fig. 2b and c are found. The effect has the expected direction (MTR_{asym} increase) for an increase in the total protein/peptide content. Therefore, we conclude that increased MTR_{asym} in the brain tumor results from increased *APTR*. Although a larger combined APT effect was detected at lower offsets, the corresponding APT images often appeared worse due to decreased signal-to-noise ratios (SNRs) for S_{sat}/S_0 and MTR_{asym} images close to the water resonance. We therefore used the APT effect of the backbone amide protons at the offset of 3.5 ppm.

Quantifying APT Contrast

As mentioned above and described in Eq. [1], the APT image contrast depends on several MR and tissue parameters. First, increased *APTR* in the tumor can be attributed either to increased cellular protein and peptide content or to increased amide proton exchange rates in the tumor with respect to the normal region. In addition, tissue water content and spin-lattice relaxation rates are two possible contributing factors. Interestingly, data in the literature (19) show that water content and R_{1w} are directly related and inversely proportional, causing partly compensated effects for water content, R_{1w}, and the exponential relaxation term in the equation. Thus, care must be taken in the interpretation of the APT contrast. The prerequisite for APT in terms of successful image contrast is that the effect of increased amide proton concentration should outweigh that of increased water content (Eq. [1]). In addition, the exchange rate of amide protons in tumor tissue should be equal to (or a little higher than) that of brain tissue to enhance the effect of increased [amide proton]. Fortunately, the data indicate that these requirements are fulfilled for healthy and tumor tissue in the present model. First, the brain water content images in Fig. 3 show limited contrast and diffuse boundaries. Second, multiple studies of many tumor types have indicated an intracellular pH (pH_i) range that is higher (up to ~0.1 pH unit) than that of normal brain tissue (31–34). As the amide proton exchange rate is base-catalyzed in the physiological pH range, the exchange rate increases with pH, thus increasing the APT contrast. These effects become clear in the MTR_{asym} (3.5 ppm) image, which is weighted by APT contrast and inherent asymmetry in the MT effect. Under the assumption of small differences in asymmetry for the MT effects of different tissues, the MTR_{asym} (3.5 ppm) images predominantly reflect the APT effect and are thus denominated as APT-weighted images.

If quantification of the amide proton content is needed, which would be valuable not only in differential diagnosis but also in noninvasive staging of disease (3,4), several parameters must be known. Equation [1] indicates that values for intracellular R_{1w} and water content are needed; however, these values are not available. We therefore used the tissue numbers for R_{1w}, and calculated water content based on R_{1w} as outlined in the Materials and Methods section. We did not measure the exchange rate for tumors in our experiments; however, since only a small pH_i increase (<0.1 pH unit) has been detected for tumors in many previous studies (31–34), we took the average proton exchange rate (28.6 s^{-1}) determined previously for normal rat brain (12) as an estimate. This was also based on the assumption of negligible effects of amide proton concentration on the exchange rate. Thus, the map for the total amide proton concentration of proteins and peptides calculated according to Eq. [1] should be viewed in terms of these assumptions. In addition, one should keep in mind that APT imaging is not sensitive to the entire protein and peptide pool, and a change in the mix of proteins and peptides that may occur in tumors with respect to the brain could bias a report of amide proton concentration.

CONCLUSIONS

Our data presented here indicate that APT imaging provides a specific and sensitive modality for tumor study by MRI. It was shown that the APT contrast in 9L gliosarcomas in rat brain depends predominantly on increased mobile protein and peptide content in the tumor, which constitutes a new type of functional MRI contrast. When it was applied to the rat brain gliosarcoma model, the technique showed a well-defined brain tumor region, whereas conventional MRI approaches showed a diffuse tumor pattern. The ability to produce image contrast in the water signal that reflects cellular protein and peptide content and amide proton exchange properties may be valuable not only for differential diagnoses, but also for the noninvasive staging of disease in clinical applications.

ACKNOWLEDGMENTS

We thank Dr. Zaver M. Bhujwalla and Dr. Martin G. Pomper for helpful discussions.

REFERENCES

1. Behar KL, Ogino T. Assignment of resonances in the ^{1}H spectrum of rat brain by two dimensional shift correlated and J-resolved NMR spectroscopy. Magn Reson Med 1991;17:285–303.

2. Kauppinen RA, Kokko H, Williams SR. Detection of mobile proteins by proton nuclear magnetic resonance spectroscopy in the guinea pig brain *ex vivo* and their partial purification. J Neurochem 1992;58:967–974.
3. Howe FA, Barton SJ, Cudlip SA, Stubbs M, Saunders DE, Murphy M, Wilkins P, Opstad KS, Doyle VL, McLean MA, Bell BA, Griffiths JR. Metabolic profiles of human brain tumors using quantitative in vivo ^{1}H magnetic resonance spectroscopy. Magn Reson Med 2003;49:223–232.
4. Srinivas PR, Srivastava S, Hanash S, Wright Jr GL. Proteomics in early detection of cancer. Clin Chem 2001;47:1901–1911.
5. Wuthrich K. NMR of proteins and nucleic acids. New York: John Wiley & Sons; 1986.
6. Mori S, Eleff SM, Pilatus U, Mori N, van Zijl PCM. Proton NMR spectroscopy of solvent-saturable resonance: a new approach to study pH effects *in situ*. Magn Reson Med 1998;40:36–42.
7. van Zijl PCM, Zhou J, Mori N, Payen J, Mori S. Mechanism of magnetization transfer during on-resonance water saturation: a new approach to detect mobile proteins, peptides, and lipids. Magn Reson Med 2003;49:440–449.
8. Chen W, Hu J. Mapping brain metabolites using a double echo-filter metabolite imaging (DEFMI) technique. J Magn Reson 1999;140:363–370.
9. Wolff SD, Balaban RS. NMR imaging of labile proton exchange. J Magn Reson 1990;86:164–169.
10. Ward KM, Aletras AH, Balaban RS. A new class of contrast agents for MRI based on proton chemical exchange dependent saturation transfer (CEST). J Magn Reson 2000;143:79–87.
11. Goffeney N, Bulte JWM, Duyn J, Bryant LH, van Zijl PCM. Sensitive NMR detection of cationic-polymer-based gene delivery systems using saturation transfer via proton exchange. J Am Chem Soc 2001;123:8628–8629.
12. Zhou J, Payen J, Wilson DA, Traystman RJ, van Zijl PCM. Using the amide proton signals of intracellular proteins and peptides to detect pH effects in MRI. Nat Med 2003;9:1085–1090.
13. Wolff SD, Balaban RS. Magnetization transfer contrast (MTC) and tissue water proton relaxation in vivo. Magn Reson Med 1989;10:135–144.
14. Bryant RG. The dynamics of water–protein interactions. Annu Rev Biophys Biomol Struct 1996;25:29–53.
15. Henkelman RM, Stanisz GJ, Graham SJ. Magnetization transfer in MRI: a review. NMR Biomed 2001;14:57–64.
16. Pekar J, Jezzard P, Roberts DA, Leigh JS, Frank JA, Mclaughlin AC. Perfusion imaging with compensation for asymmetric magnetization transfer effects. Magn Reson Med 1996;35:70–79.
17. Lal B, Indurti RR, Couraud P, Goldstein GW, Laterra J. Endothelial cell implantation and survival within experimental gliomas. Proc Natl Acad Sci USA 1994;91:9695–9699.
18. Mori S, van Zijl PCM. Diffusion weighting by the trace of the diffusion tensor within a single scan. Magn Reson Med 1995;33:41–52.
19. Lin W, Venkatesan R, Gurleyik K, He YY, Powers WJ, Hsu CY. An absolute measurement of brain water content using magnetic resonance imaging in two focal cerebral ischemic rat models. J Cereb Blood Flow Metab 2000;20:37–44.
20. Quesson B, Bouzier A-K, Thiaudiere E, Delalande C, Merle M, Canioni P. Magnetization transfer fast imaging of implanted glioma in the rat brain at 4.7T: interpretation using a binary spin-bath model. J Magn Reson Imaging 1997;7:1076–1083.
21. Ikezaki K, Takahashi M, Koga H, Kawai J, Kovacs Z, Inamura T, Fukui M. Apparent diffusion coefficient (ADC) and magnetization transfer contrast (MTC) mapping of experimental brain tumors. Acta Neurochir 1997;S70:170–172.
22. Gillies RJ, Bhujwalla Z, Evelhoch J, Garwood M, Neeman M, Robinson SP, Sotak CH, van der Sanden B. Applications of magnetic resonance in model systems: tumor biology and physiology. Neoplasia 2000;2:139–151.
23. Bhujwalla Z, Artemov D, Solaiyappan M. Insight into tumor vascularization using magnetic resonance imaging and spectroscopy. Exper Oncol 2000;22:3–7.
24. Sun Y, Carroll R, Seyfried N, Machluf M, Schmidt NO, Mulkern RV, Munasinghe J, Black P, Albert MS. MRI assessment of endostatin antiangiogenesis treatment of human brain tumors in nude mice. In: Proceedings of the 10th Annual Meeting of ISMRM, Honolulu, 2002. p 2138.
25. Cha S, Johnson G, Wadghiri YZ, Jin O, Babb J, Zagzag D, Turnbull DH. Dynamic, contrast-enhanced perfusion MRI in mouse gliomas: correlation with histopathology. Magn Reson Med 2003;49:848–855.
26. Brunberg JA, Chenevert TL, McKeever PE, Ross DA, Junck LR, Muraszko KM, Dauser R, Pipe JG, Betley AT. In vivo MR determination of water diffusion coefficient and diffusion anisotropy: correlation with structural alteration in gliomas of the cerebral hemisphere. AJNR Am J Neuroradiol 1995;16:361–371.
27. Eis M, Els T, Hoehn-Berlage M. High resolution quantitative relaxation and diffusion MRI of three different experimental brain tumors in rat. Magn Reson Med 1995;34:835–844.
28. Bastin ME, Sinha S, Whittle IR, Wardlaw JM. Measurements of water diffusion and T_1 values in peritumoural oedematous brain. Neuroreport 2002;13:1335–1340.
29. Croteau D, Scarpace L, Hearshen D, Gutierrez J, Fisher JL, Rock JP, Mikkelsen T. Correlation between magnetic resonance spectroscopy imaging and image-guided biopsies: semiquantitative and qualitative histopathological analyses of patients with untreated glioma. Neurosurgery 2001;49:823–829.
30. Nelson SJ, Graves E, Pirzkall A, Li X, Chan AA, Vigneron DB, McKnight TR. In vivo molecular imaging for planning radiation therapy of gliomas: an application of ^{1}H MRSI. J Magn Reson Imaging 2002;16:464–476.
31. Griffiths JR. Are cancer cells acidic? Br J Cancer 1991;64:425–427.
32. Ross BD, Higgins RJ, Boggan JE, Knittel B, Garwood M. ^{31}P NMR spectroscopy of the in vivo metabolism of an intracerebral glioma in the rat. Magn Reson Med 1988;6:403–417.
33. Hwang YC, Kim S-G, Evelhoch JL, Ackerman JJH. Nonglycolytic acidification of murine radiation-induced fibrosarcoma 1 tumor via 3-O-methyl-D-glucose monitored by ^{1}H, ^{2}H, ^{13}C, and ^{31}P nuclear magnetic resonance spectroscopy. Cancer Res 1992;52:1259–1266.
34. Maintz D, Heindel W, Kugel H, Jaeger R, Lackner KJ. Phosphorus-31 MR spectroscopy of normal adult human brain and brain tumors. NMR Biomed 2002;15:18–27.